Journal of Hydraulic Structures
J. Hydraul. Struct., 2023; 9(4):53-75
DOI: 10.22055/jhs.2024.44766.1264

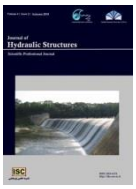

OPEN ACCESS

Investigation of the Effect of Upstream Slope and Bed Material on the Rate of Pollutant Release to Downstream Dams Using a Two-Phase SPH algorithm

Rahim Shamsoddini [1]
Bahador Abolpour [2]
Yi Zhao [3]

Abstract

Most of the pollution of dams, lakes and even coastal water is related to their upstream bed. When floods and drifts occur, the pollutants in the bed are carried into these bodies of water. There are several factors that influence the rate at which these pollutants are emitted. Among these factors, the material and slope of the bed play a crucial role, yet they have not been thoroughly investigated until now. Therefore, this study aims to model this phenomenon and examine the aforementioned parameters using a Lagrangian numerical method. The numerical method developed is the Smoothed Particle Hydrodynamics (SPH). The flow consists of two phases, one phase is considered a Newtonian fluid while the other phase is considered a non-Newtonian fluid. Due to the momentum of the fluid and the sharp changes in the flow, turbulent flow is assumed, and by approximating and calculating the turbulent viscosity, its effects are considered in the modeling. In addition to the fluid motion equations, the concentration equation is also solved to calculate the emission rate. After validating the computational code, nine different cases are modeled and evaluated based on the bed material and the slope of the bed. The results show that the change in each of these parameters has a significant effect on the emission of pollutants.

Keywords: Contamination, Angle, SPH, Two-Phase, Reservoir.

Received: 10 September 2023; Accepted: 17 February 2024

[1] Department of Mechanical Engineering, Sirjan University of Technology, Sirjan, Iran. E-mail: Shamsoddini@sirjantech.ac.ir **(Corresponding Author)**
[2] Department of Chemical Engineering, Sirjan University of Technology, Sirjan, Iran.
[3] State Laboratory of Coastal and Offshore Engineering, Dalian University of Technology, Dalian, China, 116023

1. Introduction

Public media has emphasized the potential disastrous occurrence of a landslide, which can result in the contamination of surface waters. However, there has been a lack of comprehensive scientific investigation into the pollution caused by such events. Usually, in a landslide, masses of rock, soil or debris move down the slope. Among these, debris currents are one of the most dangerous. Debris flows refer to rapid gravitational flows that are characterized by their instability and high concentration of water and solids, comprising a wide range of grain sizes. These flows usually occur without warning in mountainous areas around the world and usually cause huge human and financial losses. In general, they cause damage in three ways: deposition, erosion, and direct impact by the flow front. The destruction of the structure is frequently caused by these impacts, which is a crucial factor in both engineering design and risk assessment [1].

In their study, Göransson et al. [2] introduced an approach to assess the potential long-term ecological impacts on water bodies caused by the introduction of contaminated soil into a river as a result of a landslide. The two most common methods for investigating debris flows are the granular method and the continuum method [3]. In the present work, the continuum model with a particle-based approach is used. The method used is smoothed particle hydrodynamics (SPH). Gingold and Monaghan [4] were the pioneers in extending the application of the smoothed particle hydrodynamics (SPH) method to hydrodynamic problems. They introduced this method for the first time. On the other hand, Bøckmann et al. [5] focused on incompressible inviscid flows with free surfaces and implemented an SPH method that relied on pressure projection.

Lagrangian methods usually model sharp and sudden changes, flow break and free surface and two-phase flows more easily and accurately than Eulerian methods due to being free of fixed mesh.The SPH method is widely regarded as one of the most effective and efficient techniques for simulating free surface flows [6-8] and multiphase flows [9], owing to the inherent characteristics of the Lagrangian approach and its ability to accurately capture sudden and significant changes in the system.Therefore, it is a proper method to model the debris flows. Lagrangian methods like SPH are known to have a drawback in terms of computational speed because of the process of searching for neighboring particles in every time increment. Consequently, they are generally regarded as slow computational techniques. Hence, they are frequently employed to tackle intricate problems that Eulerian methods struggle to address or find challenging due to their complexity.

This method is widely used to simulate geophysical flows and phenomena such as floods, dam failures, landslides and movable beds. Laigle et al. [10] investigated the interactions between mudflows and structures through the utilization of SPH modeling. Crespo et al. [11] conducted a study on the behavior of dam break flow over a wet bed using the SPH method. Minatti and Pasculli [12] simulated a 2D debris flow based on a dam break-like problem along a slope using the SPH method. They used Herschel–Bulkley model to simulate the mud flow. Liang et al. [13] presented an efficient urban flood simulation by employing a GPU-accelerated SPH model. Dai et al. [1] utilized an SPH model to simulate the behavior of debris flows in the Wenjia gully and Hongchun gully. The researchers successfully predicted the movement of debris flows as well as the changes in impact forces on check dams throughout the simulation. Fathi and Ketabdari [14] used the SPH method to investigate the phenomenon of run-up and overtopping caused by solitary waves on SBW. Tayyebi et al. [15] utilized an innovative two-phase depth-integrated SPH model to simulate a debris flow. The model incorporated the influence of bed entrainment and the evolution of pore-water pressure, providing a comprehensive understanding of the flow dynamics. Mao et al. [16] conducted a study where they employed six different combinations of well-known rheological models and yield criteria,

each with distinct physical properties, within the framework of SPH. The aim of their research was to replicate four well-established erosion experiments. In their study, Zheng et al. [17] developed a macroscopic-scale two-dimensional water-sediment two-phase flow model using SPH method. The model was specifically designed to replicate the extensive sediment accumulation and propagation observed in landslides triggered by dam breaks. Shamsoddini et al. [18] using the SPH method, examined five distinct movable bed models and explored the rate at which the downstream tank is filled with these materials. The findings indicate that, within the Herschel-Bulkley model parameters, the yield stress has a greater impact compared to other factors. Goodwin et al. [19] conducted an investigation on the interaction between gravity-driven surges and mobile beds by utilizing an SPH model. their primary focus was on studying the mechanisms of entrainment. They noted that the connection between various regimes is characterized by a significantly non-monotonous behavior.

The hazards and destructive environmental effects of these currents reveal the need for further studies in this field. The volume of destruction in debris flows is greatly influenced by the kinetic energy and momentum of the fluid mass. The slope of the land is a crucial factor that affects these values, along with the physical properties of the upstream soil. According to the authors' studies, the effect of the slope of the land and the type of bed material on the level of pollution of downstream waters has not been investigated.Therefore, in the present work, the effects of land slope and bed material on the transfer of upstream material to the downstream dam are investigated. These materials can carry contaminants that contaminate downstream dam water. Hence, in the current study, the equations governing fluid motion as well as the equation governing mass transfer (concentration) are solved simultaneously.

The SPH method is employed as the solution approach, incorporating a two-phase design that takes into account the influence of the free surface and surface tension. Additionally, the impact of turbulence is accounted for by evaluating the turbulence viscosity. In the following, first, the details and equations of the numerical method are stated, and then the results are discussed.

2. Numerical procedure

This section introduces the governing equations and how to apply them in the computational code. The solution method is the SPH method, and the governing equations are the equations of mass and momentum continuity.

$$\nabla \cdot \boldsymbol{V} = 0 \tag{1}$$

$$\rho \frac{D\boldsymbol{V}}{Dt} = -\nabla p + \rho \boldsymbol{g} + \nabla . \boldsymbol{\tau} + \boldsymbol{F_s} \tag{2}$$

where ρ, t, $\boldsymbol{V}$, p, $\boldsymbol{g}$, $\boldsymbol{\tau}$, and $\boldsymbol{F_s}$ are the density, time, velocity vector, pressure, gravity acceleration, total shear stress tensor, and surface tension, respectively. In the simulation, there exist both Newtonian and non-Newtonian fluids. Therefore, the stress tensor is stated as follows:

$$\boldsymbol{\tau} = 2\mu_e \dot{\boldsymbol{\gamma}} \tag{3}$$

Where

$$\dot{\boldsymbol{\gamma}} = \frac{1}{2}(\nabla \boldsymbol{u} + (\nabla \boldsymbol{u})^T) \tag{4}$$

In the SPH method, the discretization of $\nabla \boldsymbol{u}$ can be expressed as follows:

$$\langle \nabla \boldsymbol{u} \rangle_i = \sum_j \forall_j \left(\boldsymbol{u}_j - \boldsymbol{u}_i \right) \boldsymbol{B}_i \cdot \nabla W_{ij} \tag{5}$$

The variables *i* and *j* represent the particle counter, while *W* and *B* denote the kernel function and corrective tensor, respectively.Various kernel functions have been introduced and used, one of the most appropriate of which is the fifth-order Wendland kernel function [20].

The corrective tensor $\boldsymbol{B}$ is calculated by:

$$\boldsymbol{B}_i = -\left[\sum_j \forall_j r_{ij} \nabla W_{ij} \right]^{-1} \tag{6}$$

As previously stated, the computational code can model two-phase flows, one of which can be a non-Newtonian fluid. The Herschel-Bulkley fluid is regarded as the upstream flow, referring to the flow of mud that enters the dam or natural open water reservoirs. The effective viscosity of the Herschel–Bulkley model is predicted by:

$$\mu_{f_i} = k\dot{\gamma}^{n-1} + \left(\frac{\tau_0}{\dot{\gamma}}\right)\left(1 - e^{-m\dot{\gamma}}\right) \tag{7}$$

$$\dot{\gamma} = \sqrt{2(\dot{\boldsymbol{\gamma}} : \dot{\boldsymbol{\gamma}})} \tag{8}$$

where τ_0 is the yield stress, *k* is the consistency index, and *n* is the power-law index.

$$\langle \nabla . \boldsymbol{\tau} \rangle_i = \sum_j 2\forall_j \left(\mu_{e_{ij}} \right) \frac{\boldsymbol{V}_i - \boldsymbol{V}_j}{r_{ij}} e_{ij} . \left(\boldsymbol{B}_i . \nabla W_{ij} \right) \tag{9}$$

where $\mu_{e_{ij}} = (\mu_{e_i} + \mu_{e_j})/2$and μ_{e_i} is equal to:

$$\mu_{e_i} = \mu_{f_i} + \mu_{t_i} \tag{10}$$

In which μ_{t_i} is the turbulent viscosity calculated by:

$$\mu_{t_i} = \left(\rho (c_s \delta)^2 |\overline{\boldsymbol{S}}|\right)_i \tag{11}$$

where c_s equals 0.2, δ is the particle space, and $|\overline{\boldsymbol{S}}|$ is

$$|\overline{\boldsymbol{S}}| = \sqrt{2\boldsymbol{S}_{ij} : \boldsymbol{S}_{ij}}, \tag{12}$$

in which $\boldsymbol{S}_{ij} = \dot{\boldsymbol{\gamma}}$.

Another term that may be taken into account is the acceleration due to the surface tension force. The surface tension is equal to [21-22]:

$$\boldsymbol{F}_{s_i} = \sigma \boldsymbol{\kappa_i} \delta_{s_i} \tag{13}$$

In this equation, $\boldsymbol{\kappa_i}$ is equal to:

$$\boldsymbol{\kappa_i} = \sum_j \forall_j \boldsymbol{B}_i \cdot \nabla W_{ij} \cdot \left(\boldsymbol{n}_j - \boldsymbol{n}_i\right) \tag{14}$$

where $\boldsymbol{n}_i$ is normal vector on interface surface:

$$\boldsymbol{n}_i = \frac{\nabla \tilde{C}_i}{\left|\nabla \tilde{C}_i\right|} \tag{15}$$

where $\tilde{C}$ is the normalized color function; at first, one of the phases is given the color number one, and the other is given the color number zero. The last parameter in the equation is δ_{s_i}, which is calculated by:

$$\delta_{s_i} = \left|\nabla \tilde{C}_i\right| \tag{16}$$

After calculating the shear stress and surface tension, the intermediate velocity is defined according to the following equation:

$$\boldsymbol{V}_i^{*,n+1} = \boldsymbol{V}_i^n + (\boldsymbol{g} + \frac{1}{\rho}\nabla.\boldsymbol{\tau} + \frac{1}{\rho}\boldsymbol{F_s})\Delta t \tag{17}$$

The Poisson equation can be expressed in the SPH discretization form by utilizing intermediate velocity as shown below:

$$\sum_j 2\frac{\forall_j}{\rho_{ij}}\frac{P_i^{n+1} - P_j^n}{r_{ij}} e_{ij}.\left(\boldsymbol{B}_i.\nabla W_{ij}\right) = \frac{\langle \nabla \cdot \boldsymbol{V}_i^{*,n+1}\rangle}{\Delta t} \tag{18}$$

In which $\rho_{ij} = (\rho_i + \rho_j)/2$.
After computing the pressure, the final velocity is calculated as follows:

$$\boldsymbol{V}_i^{n+1} = \boldsymbol{V}_i^{*,n+1} - \langle\frac{\nabla p}{\rho}\rangle_i^{n+1}\Delta t \tag{19}$$

Finally, the new position for all particles is calculated:

$$\boldsymbol{r}_i^{n+1} = \boldsymbol{r}_i^n + \boldsymbol{V}_i^{n+1}\Delta t \tag{20}$$

To obtain pressure on the wall, the normal surface vector is dot multiplied in the momentum equation:

$$\left(\frac{\nabla p}{\rho}\right)\cdot \boldsymbol{n}_w = \frac{1}{\rho}\frac{\partial p}{\partial n_w} = -\frac{d\boldsymbol{V}_b}{dt}\cdot \boldsymbol{n}_w + \frac{1}{\rho}(\nabla.\boldsymbol{\tau})\cdot \boldsymbol{n}_w + \boldsymbol{g}.\boldsymbol{n_w} \tag{21}$$

While the wall particles remain stationary in relation to the dummy particles, the finite difference method can be employed to discretize this equation:

$$p_i^{n+1} = p_i^n + \rho\delta_n\left(-\frac{d\boldsymbol{V}_b}{dt}\cdot\boldsymbol{n}_w + \frac{1}{\rho}(\nabla.\boldsymbol{\tau})\cdot\boldsymbol{n}_w + \boldsymbol{g}.\boldsymbol{n}_w\right) \quad (22)$$

The SPH method is plagued by failure, cluster alignment, and particle bonding as its inherent weaknesses. However, particle shifting provides a solution to these troublesome phenomena. The research conducted by Shadloo et al. [23] introduced the displacement particle algorithm, which is considered one of the groundbreaking studies in this field. To avoid the emergence of these undesirable occurrences, an algorithm for particle displacement similar to that reported by Shamsoddini and Mofidi [9] is applied and implemented; in this algorithm, first, the shifting vector is calculated by:

$$\Delta\boldsymbol{r_i} = \varepsilon\bar{\boldsymbol{r}}_{\boldsymbol{i}} \quad (23)$$

where ε is a constant factor between 0 and 0.1 and $\bar{\boldsymbol{r}}_{\boldsymbol{i}}$ is:

$$\bar{\boldsymbol{r}}_{\boldsymbol{i}} = \sum_j \forall_j \boldsymbol{r}_{ij} W_{ij} \quad (24)$$

Then, the particle is shifted by $\Delta\boldsymbol{r_i}$, and the flow field variables are corrected as follows:

$$\boldsymbol{V}_i = \boldsymbol{V}_i + \Delta\boldsymbol{V}_i = \boldsymbol{V}_i + \Delta\boldsymbol{r_i}\cdot\langle\nabla\boldsymbol{V_i}\rangle \quad (25)$$

$$\boldsymbol{p}_i = \boldsymbol{p}_i + \Delta\boldsymbol{p}_i = \boldsymbol{p}_i + \Delta\boldsymbol{r_i}\cdot\langle\nabla\boldsymbol{p_i}\rangle \quad (26)$$

In the single-phase configuration, particles positioned on the free surface experience no pressure. To identify a particle on the free surface, a distinct subroutine is developed to compute the divergence of the location vector $\nabla\cdot\boldsymbol{r}$. The value for a two-dimensional fluid flow must be equal to 2.0, ($\nabla\cdot\boldsymbol{r} = 2$). Nevertheless, as a result of the insufficient particle filling within the kernel function, the aforementioned value decreases to a value below 2.0 at the free surface. Additionally, in order to guarantee the accurate choice of the particle on the free surface, another equivalent condition is used simultaneously; for each particle: $\sum_j \forall_j W_{ij} = 1.0$. However, the aforementioned causes the fluid particle situated on the free surface to possess a value lower than one. In the present work, a particle is regarded as a free surface particle if its value is below 0.85.

The level and rate of filling dams, wetlands and lakes with upstream materials is one of the common problems that reduces the nominal volume of their reservoir. In addition, it can transfer contaminants and harmful salts and surface waste into the water. To calculate the transfer rate of soil waste pollution in water, the concentration equation is solved as follows:

$$\frac{dC}{dt} = \alpha\nabla^2 C \quad (27)$$

where SPH discretization of the above equation is:

$$C_i^{n+1} = C_i^n + \sum_{j=1}^{N} 2\forall_j\alpha_e\frac{C_i - C_j}{r_{ij}}e_{ij}\cdot\left(\boldsymbol{B}_i\cdot\nabla W_{ij}\right) \quad (28)$$

In these relationships, C is the concentration and α is the molecular diffusion coefficient of the pollutants.

There are several factors influencing this transfer phenomenon, the most important of which are the upstream slope of the reservoir and the type of soil or inlet material. Therefore, in this article, these two factors are examined.

3. Validation

The case considered for validation is the simulation of Herschel–Bulkley fluid flowing due to dam-breaking phenomenon. The findings of Minussi and Maciel [25] are employed for comparison in the context of Herschel-Bulkley dam-break flow. The initial condition of the problem consists of a liquid with a height of 10 cm, and a width of 0.5 m behind a dam where the dam wall is suddenly broken (removed) and fluid flows along the surface due to gravitational acceleration The properties of the fluid are τ_0=30.002, n=0.479, and k=4.297. This problem is also modeled in two single-phase and two-phase modes. The results of the present work in comparison with experimental results reported by Minussi and Maciel. [21] are shown in Figure-1. This figure shows the many similarities between the present numerical work and the experimental sample.

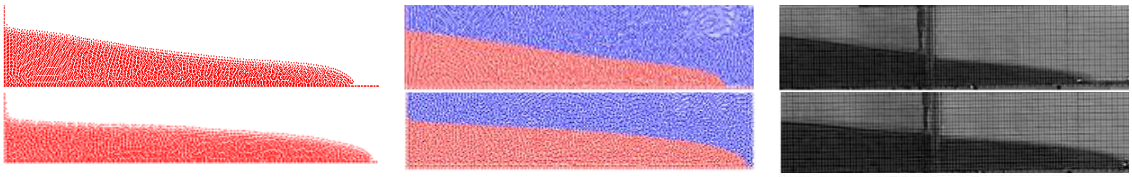

Figure 1. Comparison between numerical results in single-phase and two-phase mode with experimental results

Figure 2 shows a quantitative comparison between the results of the present work in single-phase and two-phase models with the results of Minussi and Maciel, [25]. This analysis demonstrates the suitable convergence of methods.

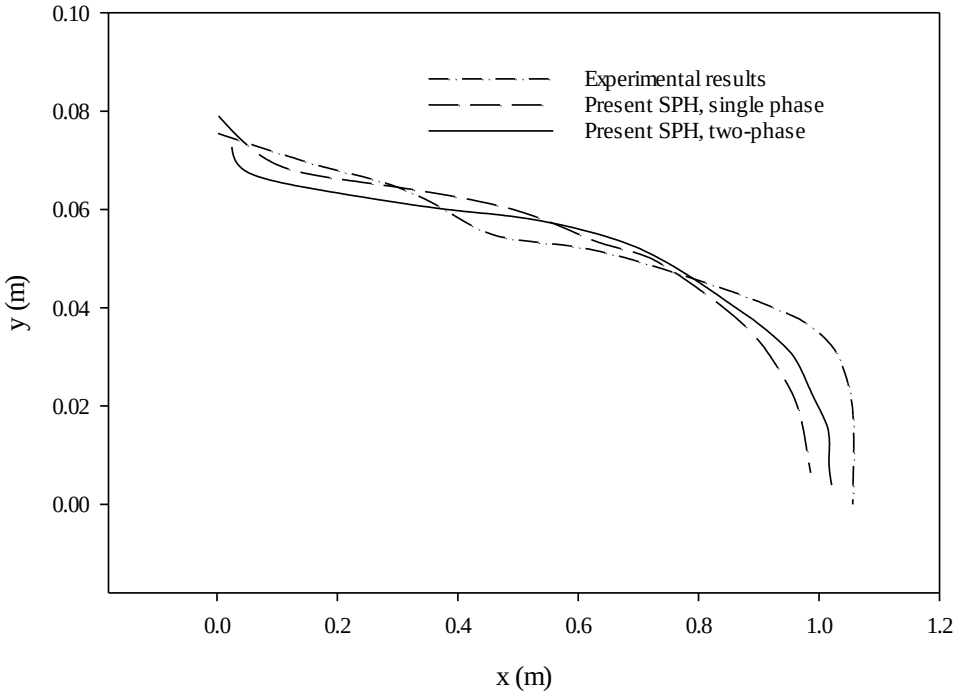

Figure 2. Quantitative comparison between numerical results in single-phase and two-phase mode with experimental results at t=1.0s.

The accuracy of the results is determined by employing standard deviation, root-mean-square error (RMSE), R-squared (R^2), and mean absolute error (MAE). Table 1, shows these values. The results show there is acceptable confirmation between the experimental and numerical results.

Table 1. table of errors including, standard davation, R^2, MAE relative to the experimental results of Minussi and Maciel, [25].

	Mean (y)	*Standard Deviation*	*RMSE*	*R^2*	*MAE*
SPH single phase (t=1.0 s)	0.0562	0.0115	0.0037	0.8824	0.0277
SPH two phase (t=1.0 s)	0.0558	0.0094	0.0039	0.8006	0.0321

Also, the present problem was validated by utilizing the experimental work conducted by Spinewine [26]. This particular problem focuses on the Dam-Break Problem occurring on a sedimentary bed. The sediment's specific density is measured at 2,683 kg/m3, while its bulk density is recorded as 1,892 kg/m3, with a friction angle of 30°, and *n*=1.0. The initial condition is presented in the first row of Table 2. Comparing the results obtained from the present code with the experimental findings of Spinewine [26], Table 2 showcases a notable concurrence between the two sets of results.

Table 2. the findings from the simulation of dam-break flow on the sedimentary bed for this study were compared to the results obtained by Spinewine [26].

	Present study	Experimental results [26]	comparison
t=0.0s	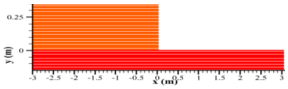		
t=0.25s	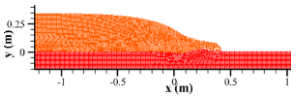		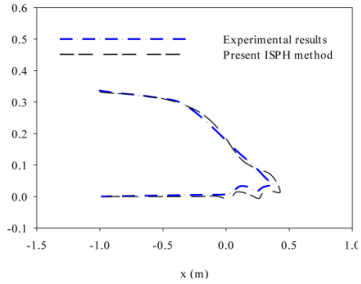
t=0.5s	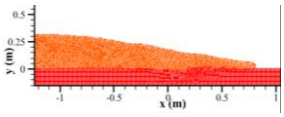		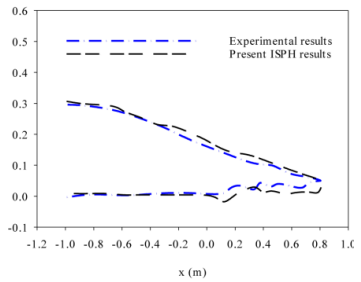

4. Problem definition

Figure 3 shows a schematic of the problem. The problem consists of two reservoirs. The upper reservoir contains discharged material, while the downstream reservoir is perceived as a dam or lake that receives the material. The upper fluid, denoted by fluid number 1, is a non-Newtonian fluid that flows from the sloping surface shown under gravity to fluid two.

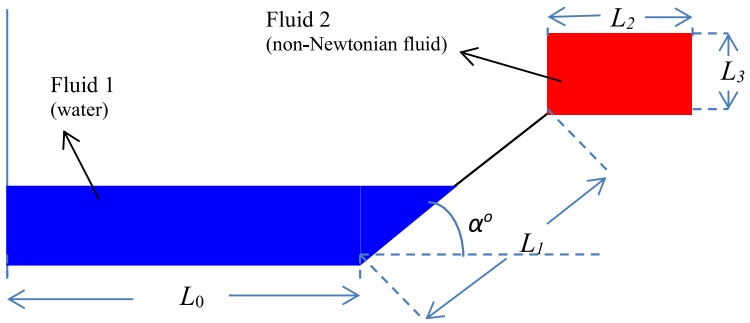

Figure 3. Definition of the problem including geometry and initial conditions. The upstream slope (α) and material of the upstream reservoir are the variables of the problem.

As mentioned, in this paper, the effect of the angle and upstream fluid material on the rate of contaminant entry (fluid 2) into water (fluid 1) is investigated. Therefore, an examination is conducted on three angles measuring 30, 45, and 60 degrees, while three distinct non-Newtonian fluids (as indicated in table 3) are selected for fluid 2. Additional geometric characteristics: The ratio of L_2 to L_3 is 2.0, while the ratio of L_0 to L_1 is 1.0 (L_2/L_3=2.0 And L_0/L_1=1.0).

Table 3. Properties of upstream materials

Case	*Bed type*	ρ	τ_0	k	n	Reference
1	Mud-clay	1165	1.26	0.22	0.47	Maciel et al. [24]
2	Mud-clay	1243	29.45	1.30	0.46	Maciel et a1. [24]
3	Mud-clay	1324	192.27	46.29	0.27	Maciel et a1. [24]

5. Results & discussion

As stated in the preceding section, an analysis is conducted on three distinct materials and three angles, resulting in a total of nine different states.The discussion is structured in such a way that three different materials will be examined in each angle.

5.1 α=30

The first angle to be examined is the 30-degree angle. The simulation results of the first case of Table 3 at a 30-degree angle are shown in Figure 4. In the first case, the fluid has very low yield stress, and after passing the yield stress due to its dilution properties, it has a strong tendency to flow. Figure 4 shows the motion of fluid 2 due to the force of gravity and its entry into fluid 1 and mixing it with fluid 1 at different dimensionless times ($t^* = t\sqrt{2g/L_1}$).

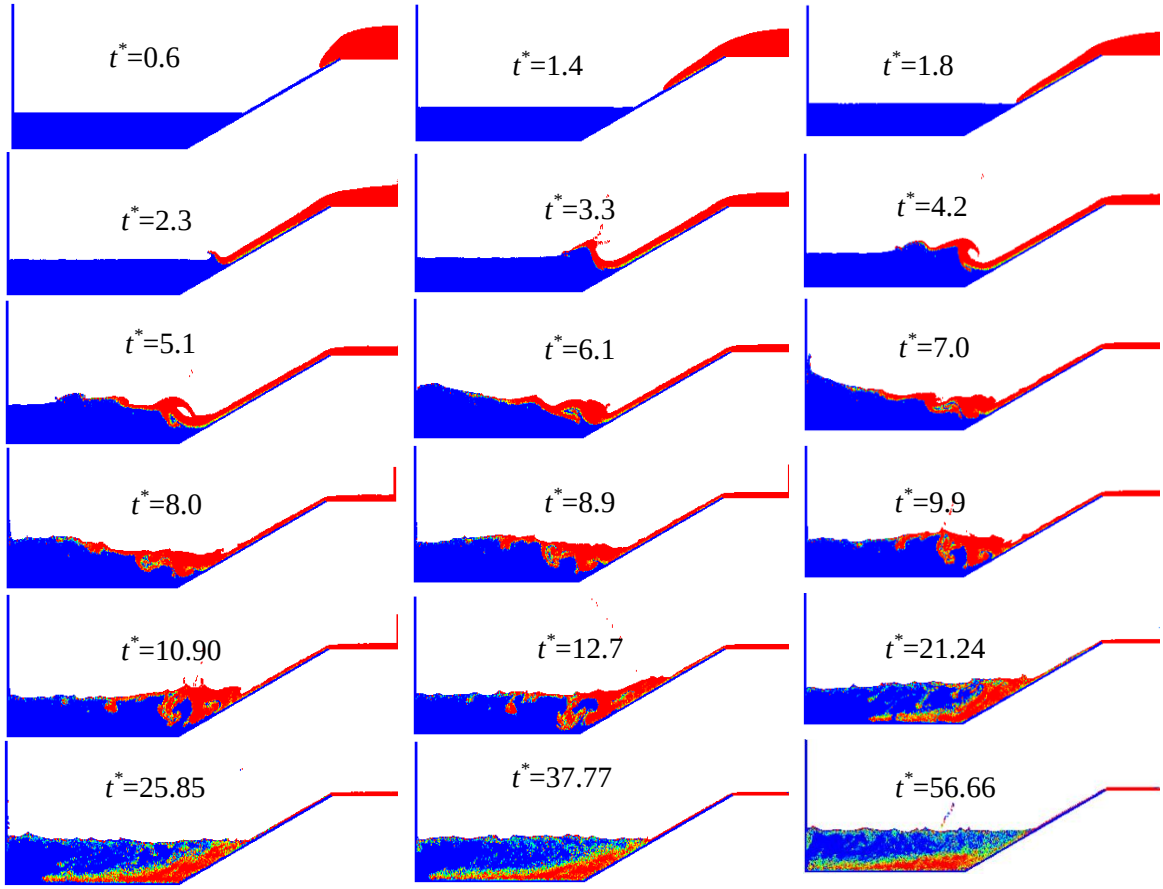

Figure 4. Simulation results for case 1 of Table 3 at θ=30°

Before t^*=1.8887, Fluid 2 has a simple motion along a sloping surface at an angle of 30-degrees, and Fluid 1 is stationary.

After this time, the interaction between the two fluids begins. Fluid 2 collides with a fluid (fluid 1) that is stationary. The effect of this collision in fluid 2 appears as a reciprocating vortex, and the formation of this vortex in the figures related to times t^*=2.3609 to t^*=5.1940 is quite evident. As the upstream momentum decreases, this vortex also becomes weaker. Fluid 2 gives a significant amount of its energy to fluid 1. The effect of this energy transfer and momentum appears as a reciprocating wave in fluid 1. The wave created in fluid 1 is evident from time t^*=2.3609, which is created on the free surface of fluid 1 and gradually grows and reaches the opposite wall at approximately time t^*=6.1383. The fluid then rises along the vertical wall (t^*=7.0827), and then the fluid return period begins. The return flow continues until t^*=12.7961 as the fluid rises along the sloping surface. The reciprocating fluid flow continues until it attains equilibrium, primarily due to fluid friction. In addition to the surface wave motion, there is another fluid displacement flow that results in a density difference between the two fluids. In addition to the surface wave motion, there is another fluid displacement flow that results in a density difference between the two fluids. Fluid 2, which is denser, is gradually transferred to the bottom of the tank and expands in the direction of the surface. Then, the main mixing mechanism is molecular diffusion. This trend is clearly traceable at times t^*=21.2481 to t^*=56.6617.

In order to quantitatively assess water pollution, it is necessary to establish a suitable metric. One such metric is the mixing index, which provides a numerical measure of the extent of pollution in water bodies [27]:

$$D_I = \sqrt{\frac{1}{N}\sum_{1}^{N}\left(\frac{C_i - C_{mean}}{C_{mean}}\right)^2} \tag{29}$$

where C_{mean} is the mean concentration (C=0.5) and N is the number of particles. The percentage of pollution is defined as follows:

$$P_p = (1 - D_I) \times 100 \tag{30}$$

According to the above formula, the amount of water pollution due to the entry of fluid 2 at time t^*=25.8587 is equal to 15%, and that at time t^*=56.6617 is equal to 25%.
The simulation results of case 2 of Table 3 at a 30-degree angle ($\alpha=30$) are shown in Figure 5.

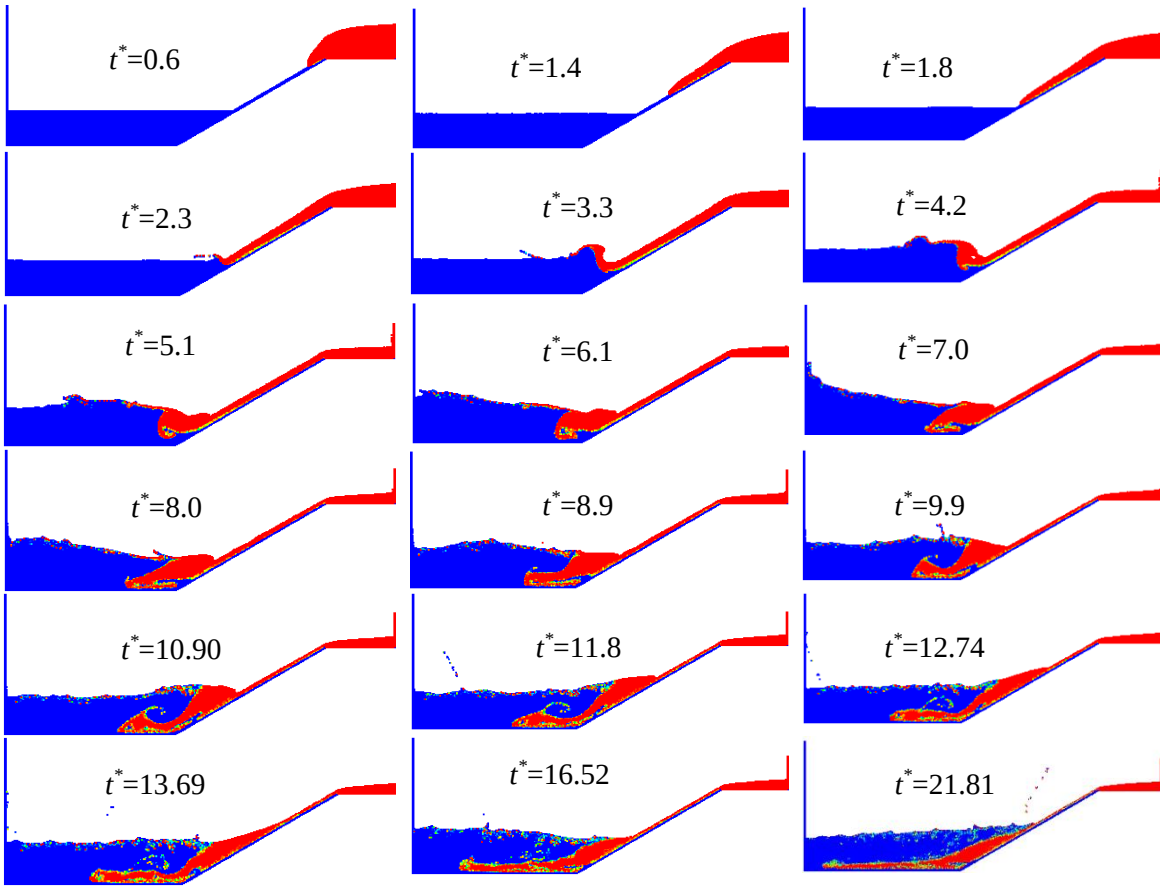

Figure 5. Simulation results for case 2 of Table 3 at θ=30°

The second case of Table 3 has more yield stress than the first mode, and its density is slightly higher. Hence, the flow behavior is slightly different. For example, the vortex that forms when fluid 2 enters fluid 1 (t^*=4.2496) is weaker and dumps faster. Additionally, due to the higher density, the process of sedimentation of fluid 2 is faster (t^*>7.0827). In comparison with the previous case, studies indicate that water pollution decreases in this case. For example, the percentage of pollution at time t^*=25 is approximately 7%, while in the previous case, it is approximately 15%.

The last case modeled at a 30-degree angle (α=30) is case 3 of Table 3. The results are shown in Figure 6. In this case, the yield stress is significantly increased. Additionally, there has been an increase in the fluid density. The high viscosity of the fluid slows down the movement of fluid 2. In this case, no vortex is formed when fluid 2 enters fluid 1. High yield stress and high fluid viscosity cause high fluid resistance to movement, the effect of which is observed at times t^*=4.2496 to t^*=35.7913. In this case, due to the low effect of the convection transfer term on the mixing phenomenon, the mixing rate is extremely low.

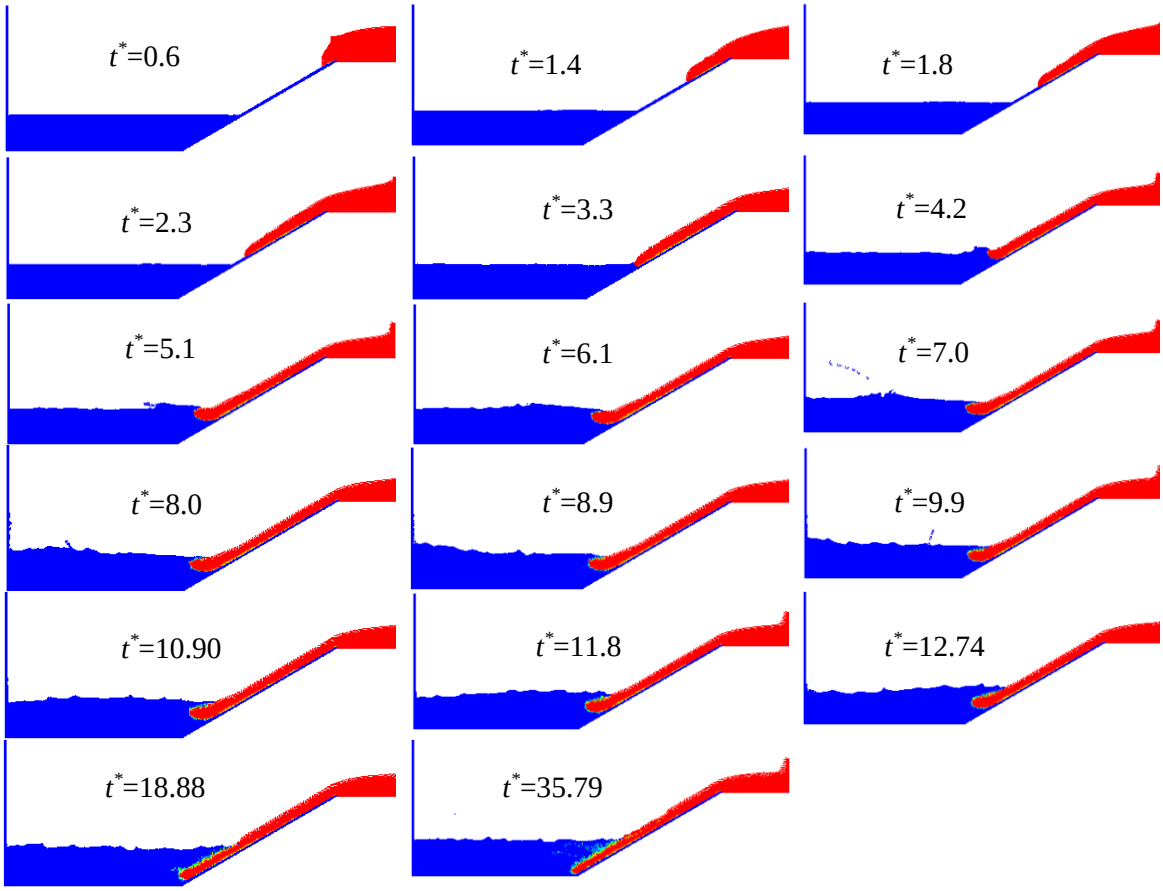

Figure 6. Simulation results for case 3 of Table 3 at θ=30°

For all three models examined at a 30-degree angle, in Figure 7, the variations in the amount of pollution over time are shown as a percentage. This figure demonstrates that the pollution rate in the first case is higher than that in the second case and that in the second case is higher than that in the third case. This indicates that as the viscosity of fluid 2 decreases, the pollution rate increases.

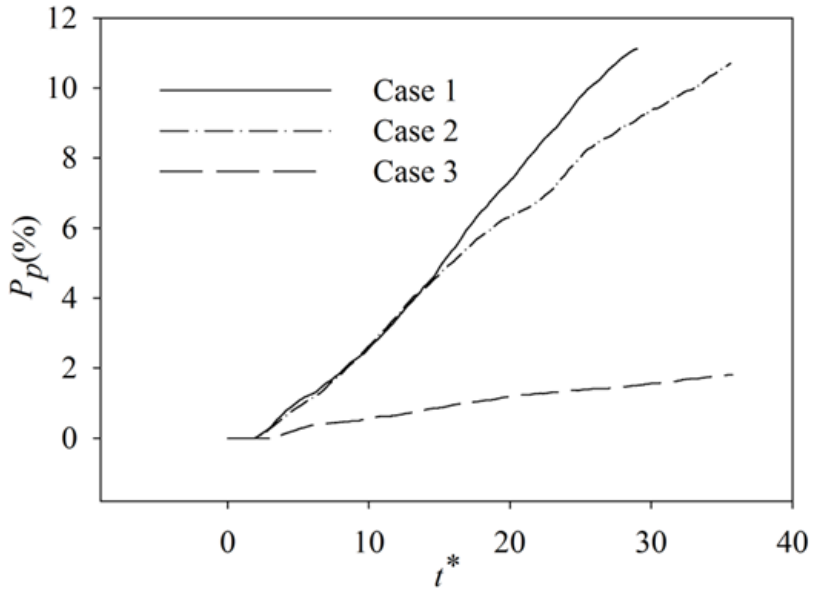

Figure 7. the variations of the amount of pollution over time for the three cases of table 3 at θ=30°

5.2 α=45

In this angle, all three cases of Table 3 are tested. The simulation results of the first case of Table 3 at this angle are shown in Figure 8. The outcomes of this mode and the 30-degree angle mode exhibit a significant resemblance in terms of the flow characteristics. In this case, the vortex created by the discharge of fluid 2 to fluid 1 has become increasingly stronger (t^*=4.2496). Hence, the vortex undergoes a prolonged dumping and dissipation process, resulting in a deceleration of fluid 2 sedimentation (compared to the same case at α=30). For this reason, the reciprocating wave created at the fluid 1 surface has become stronger and faster at t^*>2.3609.

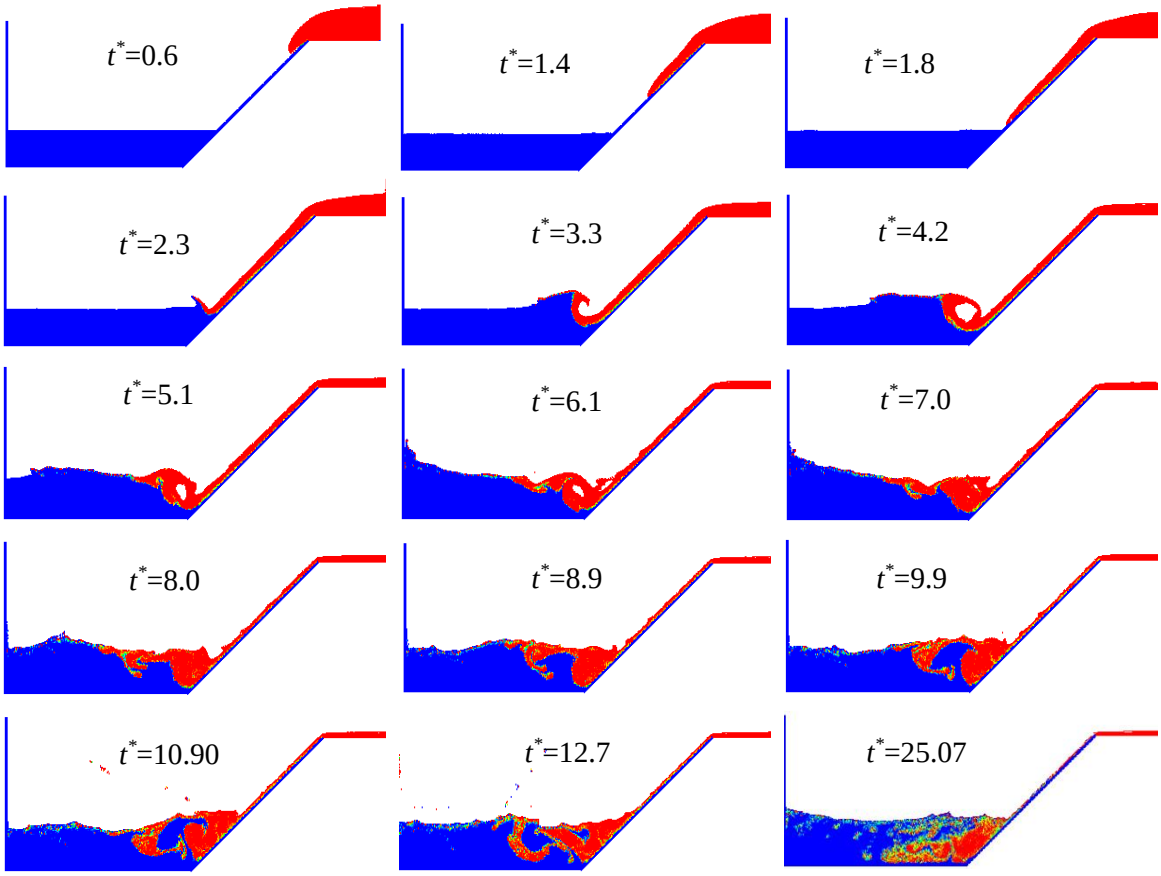

Figure 8. Simulation results for case 1 of Table 1 at θ=45°

Figure 9 shows the simulation results of the second case of Table 3 for α=45. In this case, the yield stress, viscosity, and fluid density are increased. A higher viscosity causes the vortex to dissipate faster than at the same angle (t^*=4.2496). The rate of sedimentation of fluid 2 is enhanced by increasing the density of fluid 2.

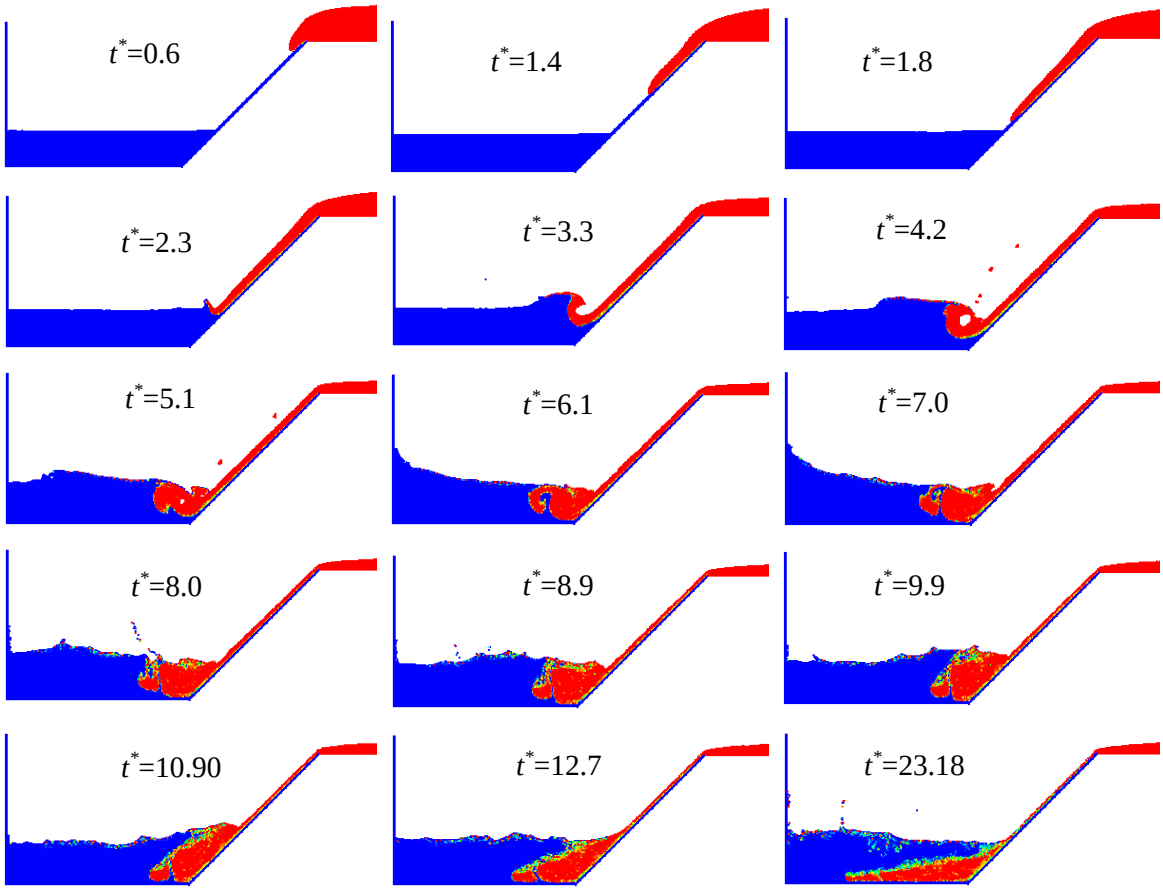

Figure 9. Simulation results for case 2 of Table 1 at θ=45°

Figure 10 shows the simulation results of the third mode of Table 3. The similarities between the temporal changes and the entry and penetration process of fluid 2 into fluid 1 depicted in this figure closely resemble those observed in Figure 6. Here, due to the high yield stress and viscosity, the motion of fluid 2 due to gravity is slow.

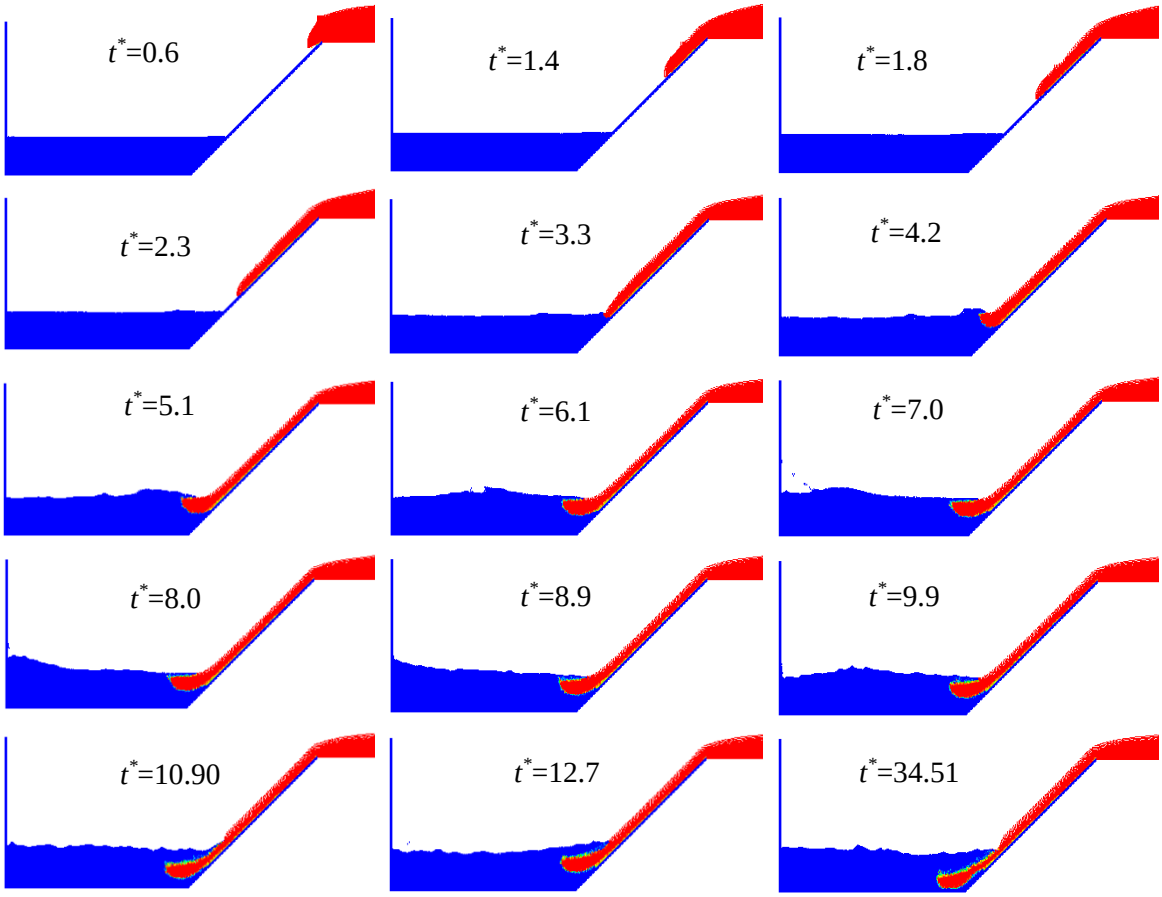

Figure 10. Simulation results for case 3 of Table 3 at θ=45°

In Figure 11, the changes in pollution percentage over time are plotted for this angle. In this figure, the trend is similar to the 30-degree angle (with increasing fluid viscosity, the pollution rate decreases). The main difference is that the differences among the cases increase.

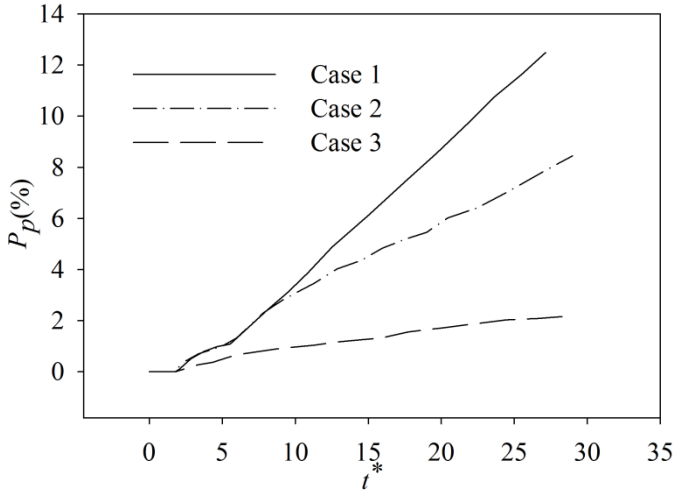

Figure 11. the variations of the amount of pollution over time for the three cases of table 3 at θ=45°

5.3 α=60

Here the surface slope increases to 60 degrees. The gravitational force component in the direction of the surface is enhanced as the angle increases, leading to a corresponding augmentation in fluid momentum. At this angle, all three states of Table 3 are simulated. Figure 12 shows the simulation results of the first case of Table 3. The size and strength of the vortex increase as fluid 2 enters fluid 1(t^*=4.2496 to t^*=8.0271). In this case, the reciprocating wave created on the fluid surface is also stronger (t^*>2.3609).

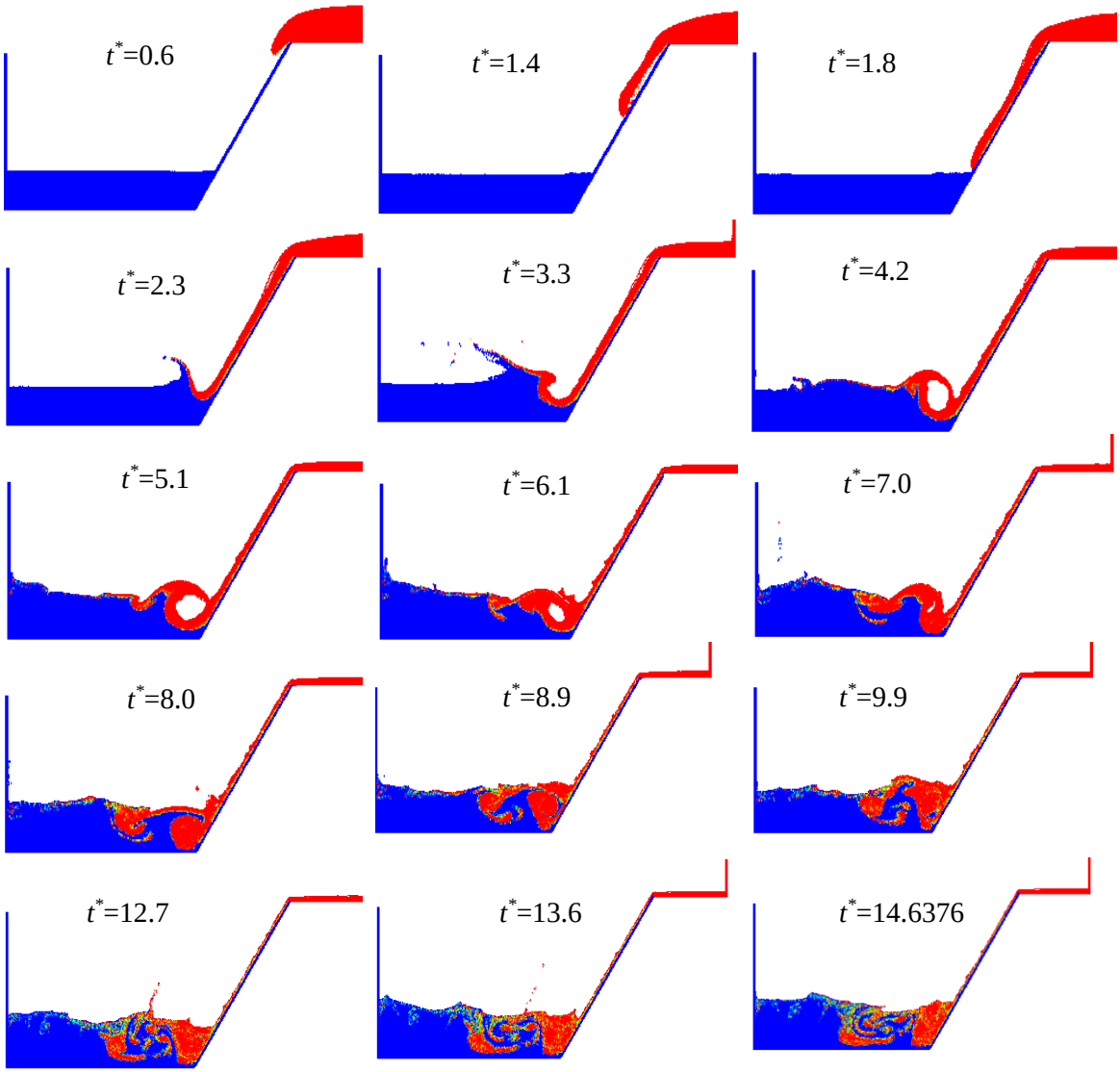

Figure 12. Simulation results for case 1 of Table 3 at θ=60°

Figure 13 also shows the simulation results of the second case of Table 3. Compared to the previous case, the tendency to settle faster is evident. The findings demonstrate the acceleration of the transfer phenomena when compared to similar scenarios at different angles.

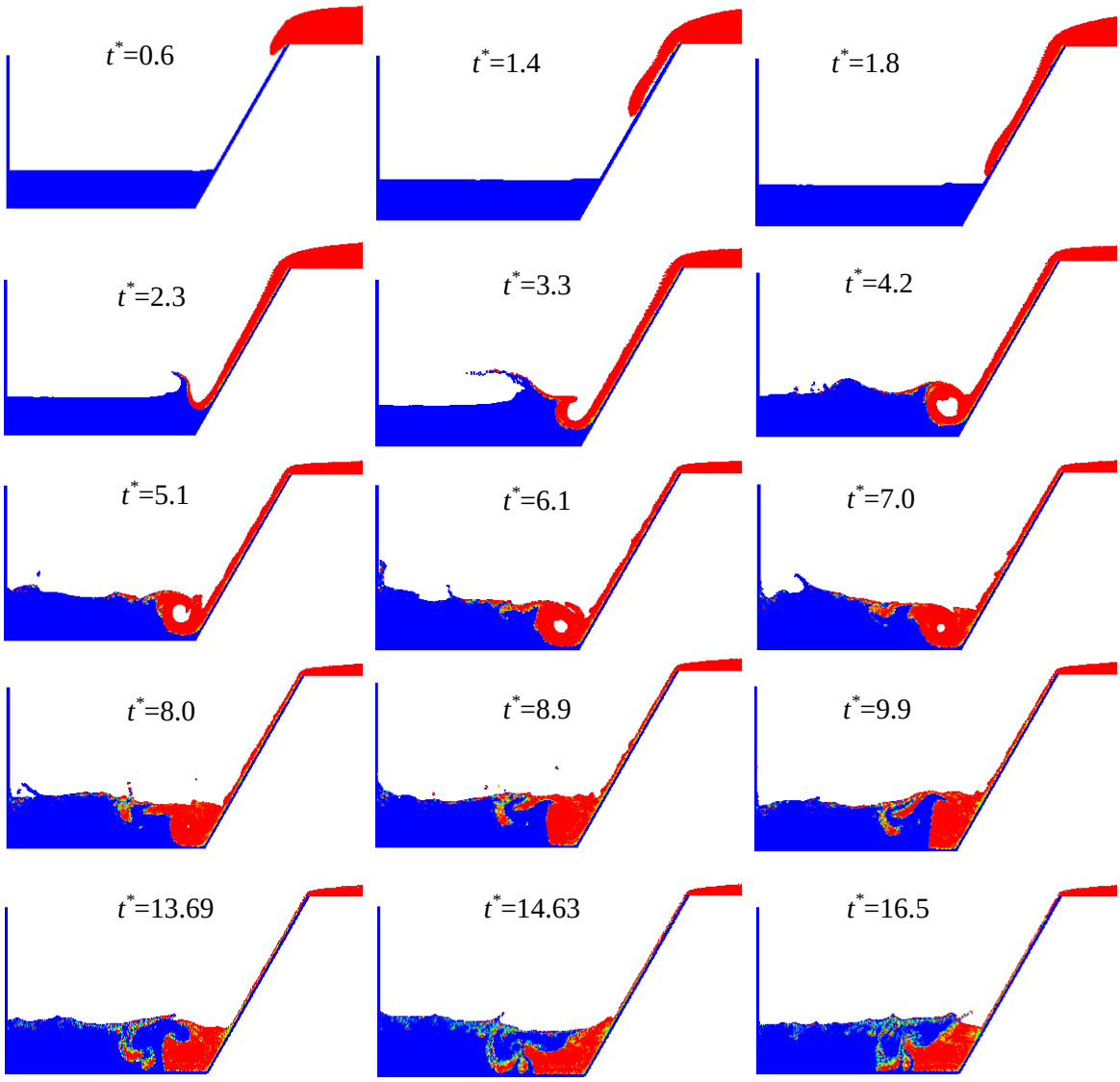

Figure 13. Simulation results for case 2 of Table 3 at θ=60°

Figure 14 shows the simulation results of the third mode of Table 3 at a 60-degree slope. In this case, although the momentum of the fluid increases due to the increase in slope, still the yield stress and high viscosity of the fluid prevent the rapid movement of fluid 2. For this reason, the mixing rate of the two fluids is much lower than that of the other two states at this angle.

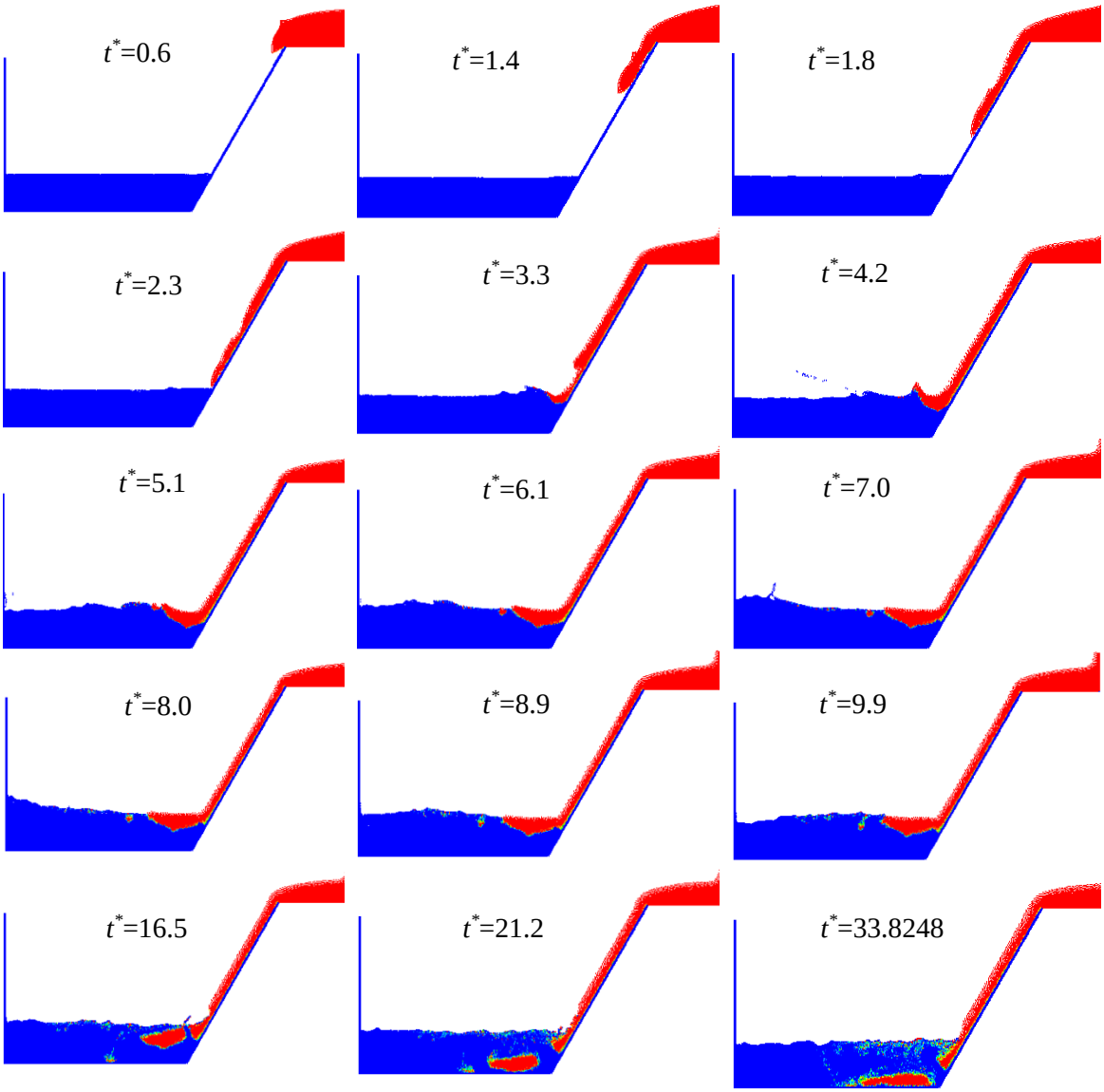

Figure 14. Simulation results for case 3 of Table 3 at θ=60°

Figure 15 shows the changes in pollution percentage over time at a 60-degree angle for all three cases studied. Here, too, the upward trend in pollution is evident as fluid 2 becomes more diluted. Additionally, compared to the previous angles, the differences among the graphs increase.

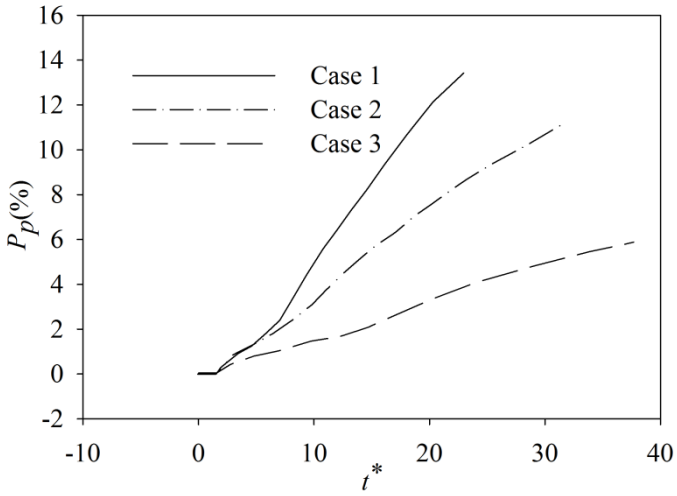

Figure 15. the variations of the amount of pollution over time for the three cases of table 3 at θ=60º

6. Conclusions

In the present work, using a Lagrangian numerical method, the effect of upstream slope and bed material on the pollutant emission to downstream dams is investigated. The numerical method used is Smoothed Particle Hydrodynamics. The flow consists of two phases, with one phase being classified as a Newtonian fluid and the other phase classified as a non-Newtonian fluid. The flow was assumed to be turbulent. In addition to the fluid motion equations, the concentration equation was also solved to calculate the emission rate. The findings of the current study can be utilized to verify the discharge of contaminants from the surface into the downstream water bodies. Three different materials are tested at three different upstream slope angles. At each angle, the pollutant emissions for the substrates were plotted and compared with different materials. The results show that the bed with high yield stress has a high resistance to flow. Even with increasing angle, it prevents the movement and release of pollutants. The rheological properties of the upstream bed are very decisive, especially the amount of yield stress. These are important in locating dams and catchments.

References

1. Dai Z, Huang Y, Cheng H, Xu Q, (2016). SPH model for fluid–structure interaction and its application to debris flow impact estimation. Landslides, pp: 14: 917-928.
2. Göransson G, Norrman J, Larson M, (2018). Contaminated landslide runout deposits in rivers–Method for estimating long-term ecological risks. Sci Total Environ, pp: 642: 553–566.
3. Pasculli A, Minatti L, Sciarra N, Paris E, (2013). SPH modeling of fast muddy debris flow: numerical and experimental comparison of certain commonly utilized approaches. Ital J Geosci, pp: 132(3):350–365.
4. Gingold RA, Monaghan JJ, (1982). Kernel estimates as a basis for general particle methods in hydrodynamics. J comput Phys, pp: 46(3): 429–453.
5. Bøckmann A, Shipilova O, Skeie G, (2012). Incompressible SPH for free surface flows. Computers & Fluids, pp: 67: 138-151.
6. Zounemat-Kermani M, Sheybanifard H, (2016). Numerical investigation of free surface flood wave and solitary wave using incompressible SPH method. J Hydraul Struct, pp: 2(2): 22-34.
7. Shamsoddini R, Aminizadeh N, (2017). Incompressible Smoothed Particle Hydrodynamics modeling and investigation of fluid mixing in a rectangular stirred tank with free surface. Chem Eng Commun, pp: 204(5): 563–572. https://doi.org/10.1080/00986445.2017.1290608.
8. Shamsoddini R, Abolpour B, (2020). Bingham fluid sloshing phenomenon modeling and investigating in a rectangular tank using SPH method. Ships Offshore Struct, pp: 1-10. https://doi.org/10.1080/17445302.2020.1748373
9. Shamsoddini R, Mofidi MR, (2021). ISPH modeling and investigation of the effect of viscosity variations on the fluids mixing in a microchannel due to oscillation of a circular cylinder. J Taiwan Inst Chem Eng, pp: 118: 78-86. https://doi.org/10.1016/j.jtice.2020.12.028.
10. Laigle D, Lachamp Ph, Naaim M, (2007). SPH-based numerical investigation of mudflow and other complex fluid flow interactions with structures. Comput Geosci, pp: 11(4): 297–306.
11. Crespo AJC, Gómez-Gesteira M, Dalrymple RA, (2008). Modeling dam break behavior over a wet bed by an SPH technique. J Waterw Port Coast, pp: 134(6): 313–320.
12. Minatti L, Pasculli A, (2011). SPH numerical approach in modeling 2D muddy debris flow. In: International Conference on Debris-Flow Hazards Mitigation: Mechanics, Prediction, and Assessment, Proceedings, pp: 467–475.
13. Liang Q, Xia X, Hou J, (2015). Efficient urban flood simulation using a GPU-accelerated SPH model. Environ Earth Sci, pp:74: 7285–7294. https://doi.org/10.1007/s12665-015-4753-4
14. Fathi A., Ketabdari MJ, (2018). Modeling of emerged semi-circular breakwater performance against solitary waves using SPH method. J Braz Soc Mech Sci Eng, pp: 40, 290. https://doi.org/10.1007/s40430-018-1179-4
15. Tayyebi SM, Pastor M, Stickle MM, (2021). Two-phase SPH numerical study of pore-water pressure effect on debris flows mobility: Yu Tung debris flow. Comput Geotech, pp: 132: 103973.
16. Wendland H, (1995). Piecewise polynomial, positive definite and compactly supported radial functions of minimal degree. Adv Comput Math, pp: 4(1): 389–396.

17. Shadloo MS, · Zainali A, · Yildiz M, (2013). Simulation of single mode Rayleigh–Taylor instability by SPH method. Comput Mech, pp: 51:699–715. https://doi.org/10.1007/s00466-012-0746-2
18. Fatehi R, Shadloo MS, Manzari MT, (2014). Numerical investigation of two-phase secondary Kelvin–Helmholtz instability. Proc Inst Mech Eng Part C, pp: 228(11): 1913-1924. https://doi.org/10.1177/0954406213512630
19. Shadloo MS, Zainali A, Sadek SH, Yildiz M, (2011). Improved incompressible smoothed particle hydrodynamics method for simulating flow around bluff bodies. Comput Methods Appl Mech Eng, pp: 200: 1008–1020. https://doi.org/10.1016/j.cma.2010.12.002.
20. Maciel GF, Santos HK, Ferreira FO, (2009). Rheological analysis of water clay compositions to investigate mudflows developing in canals. J Braz Soc Mech Sci Eng, pp: 31: 64-74
21. Minussi RB, Maciel GF, (2011). Numerical Experimental Comparison of Dam Break Flows with non-Newtonian Fluids. J Braz Soc Mech Sci] Eng, pp: 34(2): 167-178.
22. Spinewine, B. (2005). Two-layer flow behaviour and the effects of granulardilatancy in dam-break inducedsheet-flow. Ph.D. thesis, Univ. de Louvain,Louvain,Belgium.
23. Shamsoddini R, SefidM, (2015). Lagrangian simulation and analysis of the power-law fluid mixing in the two-blade circular mixers using a modified WCSPH method. Pol J Chem Tech, pp: 17: 1-10